(2)

AD

TECHNICAL REPORT ARCCB-TR-90034

AD-A230 901

A COMPARISON OF EXPERIMENTAL AND NUMERICAL BLAST DATA FOR PERFORATED MUZZLE BRAKES

G. C. CAROFANO

DECEMBER 1990

US ARMY ARMAMENT RESEARCH,
DEVELOPMENT AND ENGINEERING CENTER
CLOSE COMBAT ARMAMENTS CENTER
BENÉT LABORATORIES
WATERVLIET, N.Y. 12189-4050

APPROVED FOR PUBLIC RELEASE; DISTRIBUTION UNLIMITED

DISCLAIMER

The findings in this report are not to be construed as an official Department of the Army position unless so designated by other authorized documents.

The use of trade name(s) and/or manufacturer(s) does not constitute an official indorsement or approval.

DESTRUCTION NOTICE

For classified documents, follow the procedures in DoD 5200.22-M, Industrial Security Manual, Section II-19 or DoD 5200.1-R, Information Security Program Regulation, Chapter IX.

For unclassified, limited documents, destroy by any method that will prevent disclosure of contents or reconstruction of the document.

For unclassified, unlimited documents, destroy when the report is no longer needed. Do not return it to the originator.

SECURITY CLASSIFICATION OF THIS PAGE (When Data Entered)

REPORT DOCUMENTATION PAGE		READ INSTRUCTIONS BEFORE COMPLETING FORM
1. REPORT NUMBER ARCCB-TR-90034	2. GOVT ACCESSION NO.	3. RECIPIENT'S CATALOG NUMBER
4. TITLE (and Subtitle) A COMPARISON OF EXPERIMENTAL AND NUMERICAL BLAST DATA FOR PERFORATED MUZZLE BRAKES		5. TYPE OF REPORT & PERIOD COVERED Final 6. PERFORMING ORG. REPORT NUMBER
7. AUTHOR(s) G.C. Carofano		8. CONTRACT OR GRANT NUMBER(s)
9. PERFORMING ORGANIZATION NAME AND ADDRESS U.S. Army ARDEC Benet Laboratories, SMCAR-CCB-TL Watervliet, NY 12189-4050		10. PROGRAM ELEMENT, PROJECT, TASK AREA & WORK UNIT NUMBERS AMCMS No. 6111.02.H6100.011 PRON No. 1A04Z0CANMSC
11. CONTROLLING OFFICE NAME AND ADDRESS U.S. Army ARDEC Close Combat Armaments Center Picatinny Arsenal, NJ 07806-5000		12. REPORT DATE December 1990 13. NUMBER OF PAGES 22
14. MONITORING AGENCY NAME & ADDRESS(if different from Controlling Office)		15. SECURITY CLASS. (of this report) UNCLASSIFIED 15a. DECLASSIFICATION/DOWNGRADING SCHEDULE

16. DISTRIBUTION STATEMENT (of this Report)

Approved for public release; distribution unlimited.

17. DISTRIBUTION STATEMENT (of the abstract entered in Block 20, if different from Report)

18. SUPPLEMENTARY NOTES

Presented at the Sixth U.S. Army Symposium on Gun Dynamics, Tamiment, PA, 15-17 May 1990.
Published in Proceedings of the Symposium.

19. KEY WORDS (Continue on reverse side if necessary and identify by block number)

Muzzle Brake
Perforated Muzzle Brake
Internal Ballistics
Muzzle Blast
Numerical Blast Computation

20. ABSTRACT (Continue on reverse side if necessary and identify by block number)

In an earlier study, a numerical model of the blast field produced by a cannon having a perforated muzzle brake was given. The results compared favorably with the near-field shadowgraph data of Dillon for a 20-mm cannon. This report describes improvements to the model and compares the predictions with free-field blast data for small and large caliber cannon. The results show good agreement with data for a 20-mm cannon and satisfactory agreement with data for 105-mm and 120-mm cannon.

(CONT'D ON REVERSE)

DD FORM 1 JAN 73 1473 EDITION OF 1 NOV 65 IS OBSOLETE

UNCLASSIFIED

SECURITY CLASSIFICATION OF THIS PAGE (When Data Entered)

20. ABSTRACT (CONT'D)

Some preliminary work on a method of reducing the blast levels near the breech using upstream venting is also presented. The scheme consists simply of moving one or two rows of vents about ten calibers upstream of the muzzle. The disturbance produced by the upstream vents interferes with that produced by the remainder of the brake such that the blast levels are reduced near the breech and increased somewhat near the muzzle.

TABLE OF CONTENTS

TABLES

LIST OF ILLUSTRATIONS

INTRODUCTION

A perforated muzzle brake consists simply of a set of vents drilled through the wall of a cannon near the muzzle (see Figure 1). Venting reduces the axial thrust produced by the gas at the muzzle, thereby effecting a decrease in weapon impulse. However, the redirected exhaust increases the blast levels upstream of the muzzle. From a designer's perspective, the problem is to choose a cannon-brake system which yields specified values of muzzle velocity and weapon impulse but minimizes the blast increase.

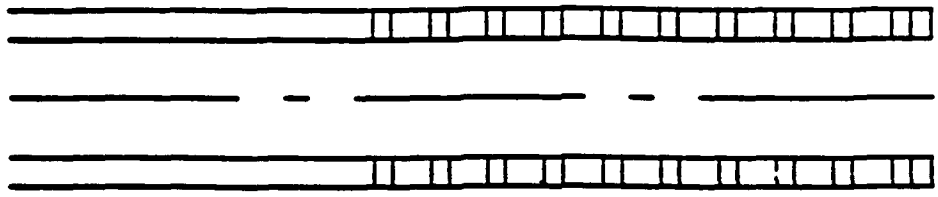

Figure 1. Schematic drawing of a perforated muzzle brake.

The magnitude of the weapon impulse was extensively studied by Dillon (refs 1,2), Dillon and Nagamatsu (refs 3-5), Nagamatsu et al. (refs 6,7), and Carofano (ref 8). References 1 through 5 also contain shadowgraph and free-field overpressure data which characterize the blast field surrounding the cannon.

The computation of the blast field is challenging because the flow is transient, three-dimensional, and must be computed to distances considerably beyond the breech if realistic pressure histories near the breech are to be obtained for reasonable periods of time. The time requirement is necessary because the peak pressure at a particular location is not always achieved in the initial portion of the blast wave. To render the calculation tractable, Carofano (ref 9) exploited a number of features of the flow. A brief description follows (see also References 6 and 8).

When the propellant gas expands through the brake, an asymmetric pressure distribution develops in each vent with the highest pressures acting on the downstream surface. To calculate the blast field, the flow through each vent is required at each instant of time during tube blowdown. Because the flow is three-dimensional, it is not practical to obtain the complete solution with a transient calculation. Fortunately, the flow contains many features which permit a vigorous simplification of the problem.

First, because of the large volume of the gun tube, the blowdown process takes on the order of tens of milliseconds, while the three-dimensional calculations indicate that the flow in a vent is established in a fraction of a millisecond. Therefore, the latter can be treated as quasi-steady and only the flow inside and outside of the tube must be considered as time-dependent.

Secondly, in the applications of interest, the flow is supersonic as it enters the brake and, due to the venting, it expands to higher Mach numbers as it travels downstream. Also, because of the high tube pressures, the gas exits each hole at near sonic or supersonic velocities over most of the exit plane area. Experience has shown that the flow is rather insensitive to the outflow boundary condition over the remaining subsonic portion. Thus, the flow at a particular vent location is not influenced by events occurring farther downstream or outside of the tube. It depends solely on the conditions in the tube upstream of the vent. In particular, it was shown (refs 6,8,9) that the flow is completely described by the upstream Mach number, the specific heat ratio and the covolume of the gas, and the vent geometry. One solution with these parameters specified is valid for all upstream pressures and densities. Thus, while a wide range of physical states are encountered during blowdown, only a few three-dimensional solutions are required to describe them.

Data from these solutions are used to obtain average values of density and pressure along with the mass and momentum fluxes in the exit plane of the vent. The averages are dimensionless functions of the parameters that appear in the three-dimensional solutions and are used to couple the interior and exterior flows.

The transient flow inside of the tube is calculated using the one-dimensional Euler equations with a source term included to represent the venting at the tube wall. This is constructed from the mass flux function and the local conditions prevailing in the tube at a given instant.

The transient flow outside of the tube is treated as axisymmetric. The large number of vents typical of such brakes and their symmetrical placement around the tube makes this feasible. Since the area of each vent represents only a portion of the local tube area, the averaged variables at the vent exit have to be adjusted to provide an appropriate boundary condition for the axisymmetric equations. A control volume approach to achieve this is described in Reference 9. The quantities at the vent exit are related to the interior flow through the averaged functions described above. Because the vent exit flow is supersonic, the exterior boundary condition is completely determined by the local conditions in the tube.

The model (ref 9) produced results which compared favorably with previously unpublished shadowgraphs of the near-field obtained by Dillon in his 20-mm experimental program. A quantitative comparison is made below of free-field overpressure data from that program taken at 30 calibers from the muzzle.

Some changes have been made in the original model to make it more generally applicable to cannon designs of current interest. For example, the perfect gas equation was replaced by the Abel equation of state to more adequately represent

the gases at the pressure levels which prevail in large caliber cannon. Also, the projectile equation of motion was added to more realistically simulate the flow discharging to the environment. Previously, the projectile was restricted to move at a constant velocity.

Finally, a distribution of vents of variable diameter and spacing can now be accommodated. This is necessary in large caliber cannon analysis where the diameters of the vents near the brake entrance may have to be smaller than those near the muzzle to avoid exceeding allowable stress levels. It was also needed to simulate the upstream venting scheme discussed below.

INITIAL CONDITIONS

The starting configuration is shown in Figure 2. The initial projectile position is chosen such that the precursor shock is located just upstream of the vented region. The state of the air between the shock and the projectile is taken to be uniform and is computed from the projectile velocity at this instant. The latter is taken from the output of a standard ballistics solution.

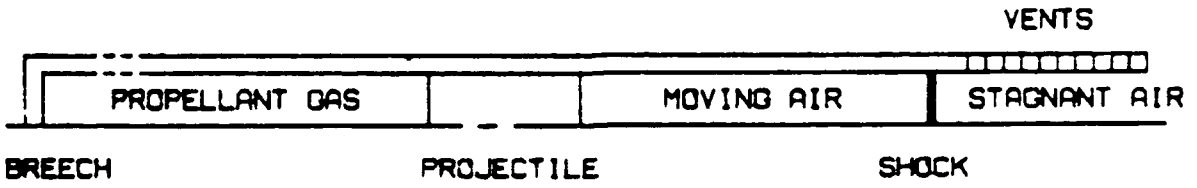

Figure 2. Starting configuration showing projectile pushing shock into the vented region.

The specification of the state of the propellant gas behind the projectile is delayed until its base reaches the vented region. During this interval, an analytical representation of the velocity and position time histories, taken from the ballistics solution, is used to advance the projectile and drive the numerical solution downstream of it. The propellant gas properties are then

calculated from the Pidduck-Kent limiting solution for an Abel gas (ref 10) using the ballistics data summarized in Table I (see References 6 and 8 for more details). In this manner, essentially all of the information generated by the ballistics solution relating to the combustion, friction, and heat transfer processes is included in the starting data behind the projectile.

TABLE I. STARTING DATA FOR PROPELLANT GAS

Parameter/Cannon	20-mm	105-mm	120-mm
Propellant mass, kg	0.0389	5.92	6.26
Projectile mass, kg	0.0980	5.79	13.45
Projectile velocity, m/sec	1045.0	1466.1	1143.3
Projectile base pressure, atm	287.0	798.0	660.1
Projectile base position, cm	143.0	427.5	402.0
Projectile base travel, cm	154.84	475.0	485.1
Bore diameter, cm	2.0	10.5	12.0
Gun chamber volume, cm^3	41.7	6472.9	8749.9
Specific heat ratio	1.25	1.24	1.23
Covolume, cm^3/kg	982.0	1050.0	1035.0
Vent area ratio of brake	6.69	4.76	3.69

A comment is necessary regarding the starting data in Table I for the 20-mm cannon. The vents were actually part of an 11.84-cm extension rather than integral with the tube. In the bare muzzle case then, the projectile base travel was only 143.0 cm. The precursor shock was initially placed at the muzzle rather than upstream, as depicted in Figure 2, and the propellant gas properties were specified when the projectile base reached the muzzle.

VENT PATTERNS

Each brake had 12 columns of vents uniformly spaced around the tube circumference (columns run parallel to the tube axis). One column for each brake is shown schematically in Figure 3. All dimensions are scaled by the cannon bore diameter to facilitate comparison. The vent area ratio, defined as the ratio of the total vent area to the cannon bore area, is given as the last entry in Table I.

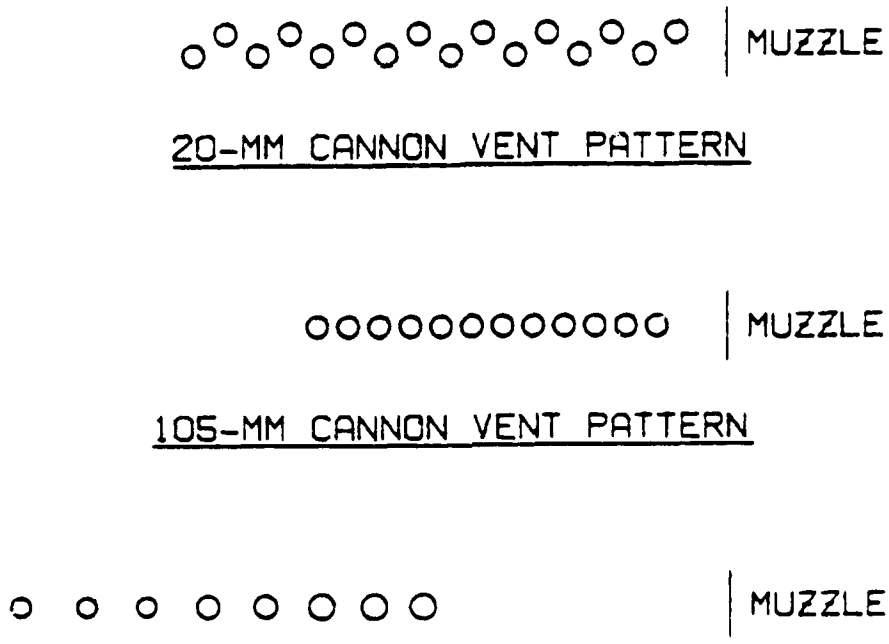

Figure 3. Vent pattern for each cannon.

In the 20-mm brake, every other hole was offset by 15 degrees in the circumferential direction to produce a staggered pattern. The code considers only the vent area per unit length of tube so the effect of staggering cannot be estimated. Presumably, this arrangement is more likely to produce the axisymmetric flow field assumed in the model than the straight patterns.

Vents of variable diameter and spacing were used in the 120-mm brake to avoid exceeding allowable stress levels. This feature is considered by the code.

A more complete description of the experimental setup for the 20-mm cannon, including a photograph of the brake, is given in Reference 1. Further details of the 105-mm and 120-mm tests are given in References 11 and 12, respectively.

CALCULATIONS

Harten's Total Variation Diminishing scheme (ref 13) was used in conjunction with a time-splitting algorithm (ref 14) to solve the Euler equations. The calculations were performed on a Cray X-MP/48 computer using a single processor. A major effort was made to exploit the vector hardware wherever possible.

A uniform grid was employed over a rectangular region extending 60 calibers upstream from the muzzle, 110 calibers downstream, and 70 calibers radially outward from the tube axis. Beyond this region, a gradually expanding grid was used to limit memory requirements while still permitting the calculation to continue. Four cells were used across the tube radius, 800 in the axial direction and 350 in the radial direction. The program required 1.6 megawords of memory for these array sizes.

The size of the active grid is determined at the beginning of each time step to eliminate computation in the undisturbed environment. Run times for each configuration are given in Table II. More time steps are required for the bare muzzle cases because the disturbance which propagates upstream takes longer to reach the pressure gages (see next section).

TABLE II. COMPUTATION TIMES

Cannon	Time Steps	CPU Minutes
20-mm, bare muzzle	1200	38.8
20-mm, with brake	1000	25.0
105-mm, bare muzzle	1200	38.6
105-mm, with brake	1000	28.5
120-mm, bare muzzle	1200	37.8
120-mm, with brake	1000	26.6

PRESSURE CONTOUR PLOTS

The blast fields produced by each cannon after 600 time steps are shown in Figures 4 through 6. Each plot is scaled by the respective cannon bore diameter to facilitate comparison. The small circles, located on a radius 30 calibers from the muzzle, indicate where pressure histories were stored in the calculations or measured in the experiments. Note in Figure 4, that when the brake extension was added in the 20-mm experiment, the gages were left at the positions they occupied in the bare muzzle case.

The principal effect of venting is seen to be the generation of a more uniform blast field around the cannon. The disturbance is diminished somewhat downstream of the muzzle and considerably strengthened upstream.

The 20-mm cannon had a significantly higher ratio of travel length to bore diameter than either large cannon. This produced a precursor flow of relatively long duration ahead of the projectile. In Figure 4, remnants of the precursor shock can be seen upstream of the muzzle and near the 60-degree gage position in the brake case. The precursor shock is completely overtaken by the main blast wave for both large cannon because of their relatively shorter barrels.

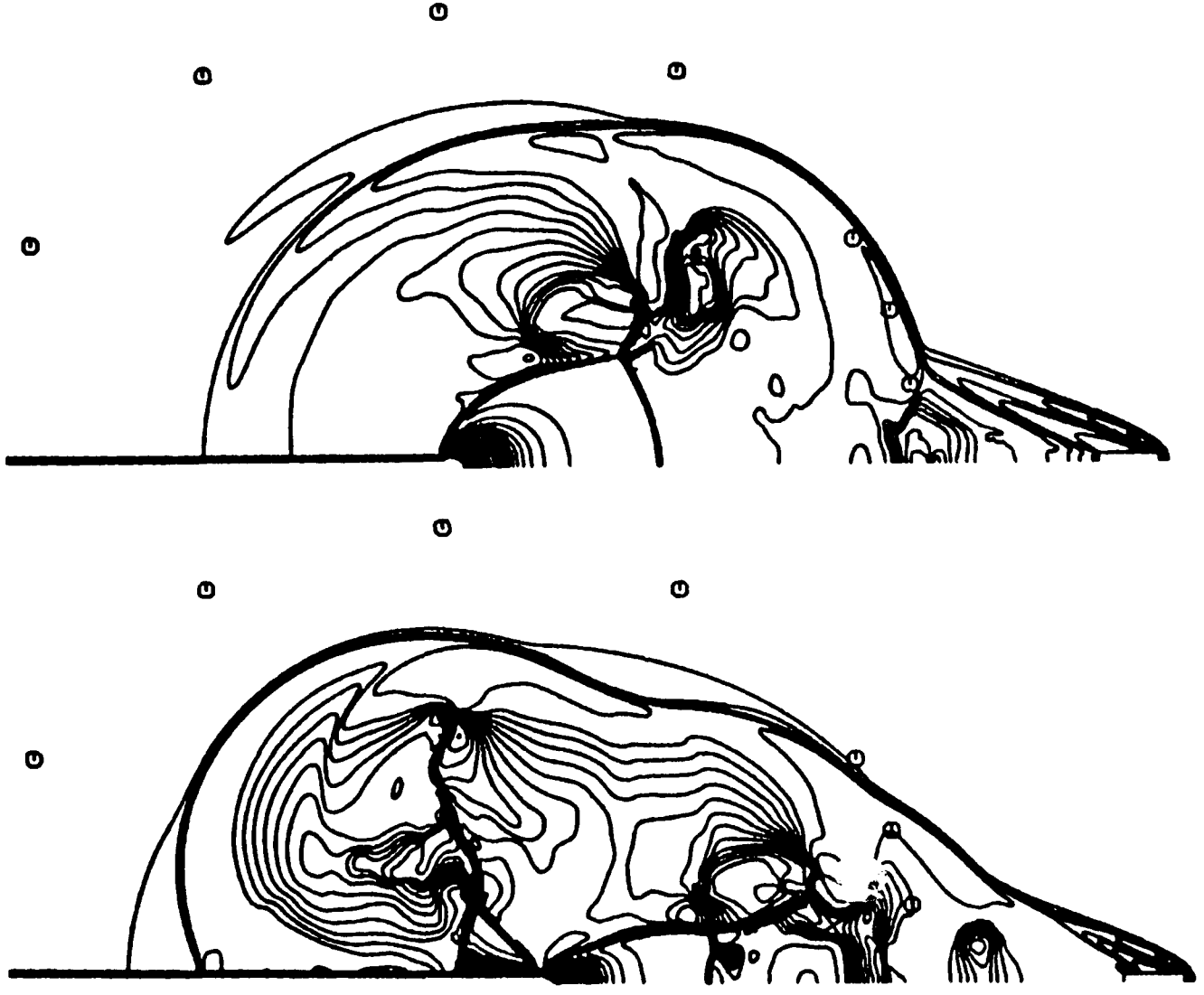

Figure 4. Pressure contour plots for the 20-mm cannon with and without venting.

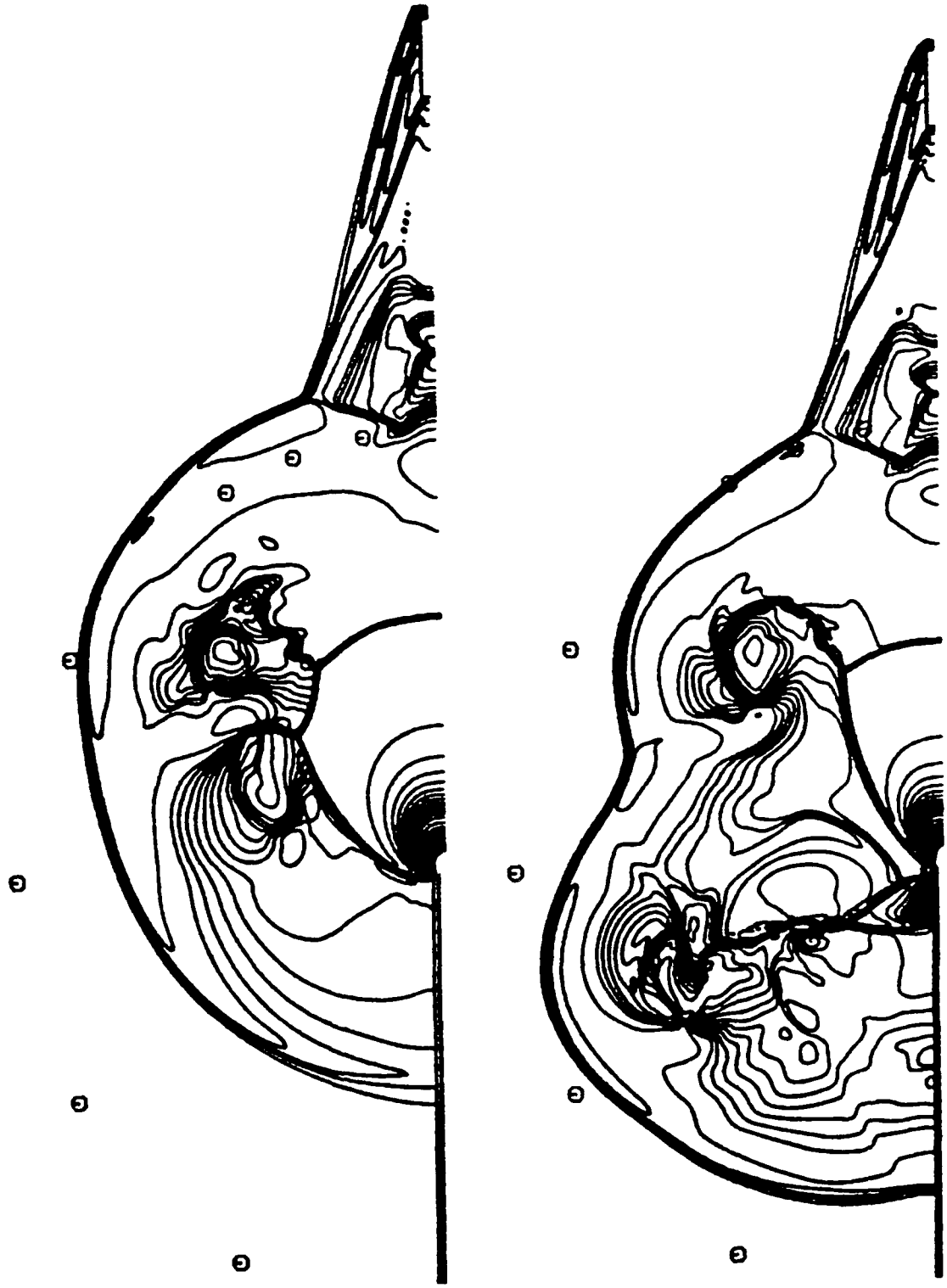

Figure 5. Pressure contour plots for the 105-mm cannon with and without venting.

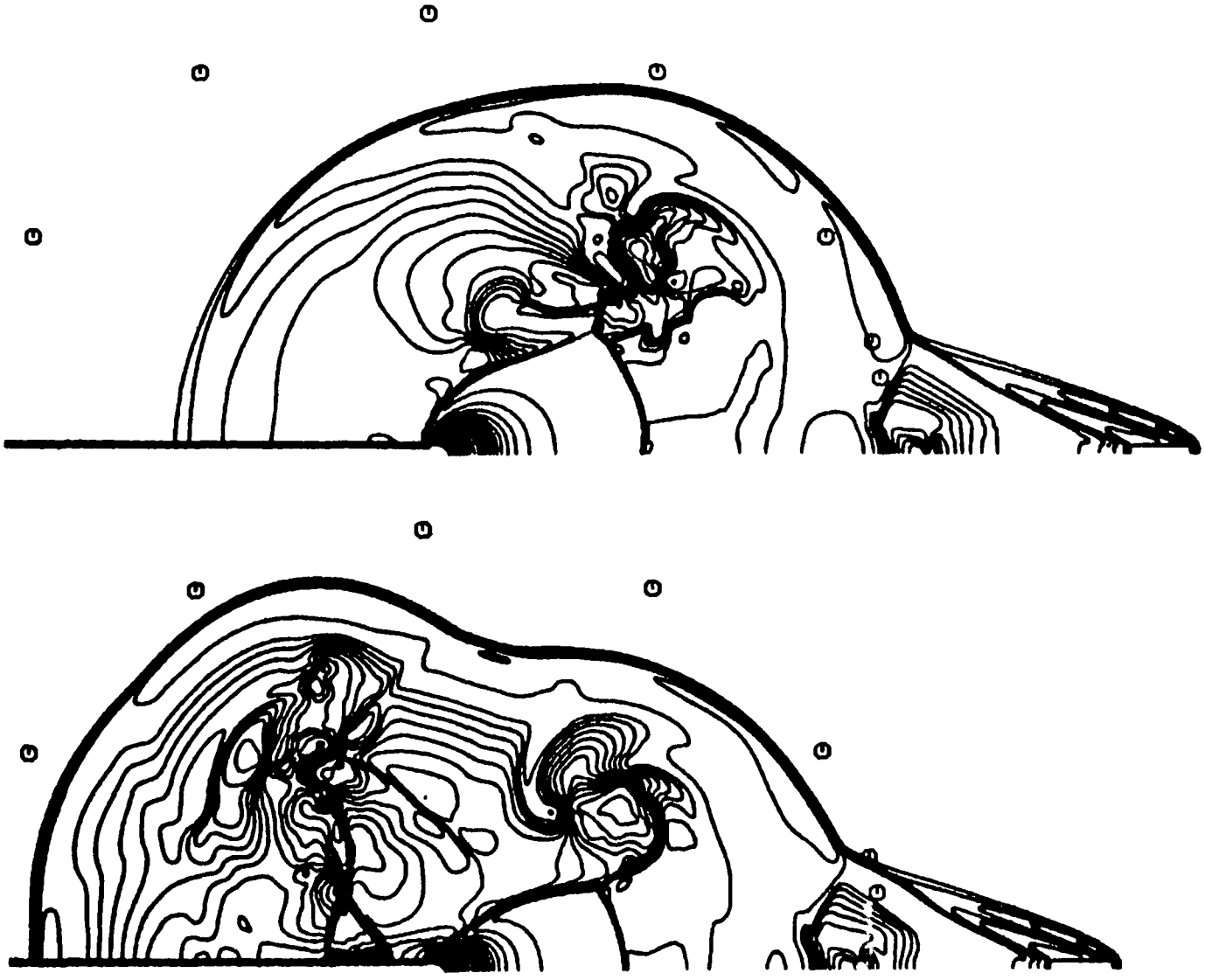

Figure 6. Pressure contour plots for the 120-mm cannon with and without venting.

What other differences exist in the various blast fields are due mainly to the variations in projectile base pressure and velocity or the brake geometry. Some 20-mm experiments are planned that will employ brakes which are geometrically similar to those being used in ongoing 105-mm and 120-mm tests. The question of scaling the blast field will be addressed when these data become available.

OVERPRESSURE RESULTS

In Figure 7, experimental free-field overpressure data are given for the 20-mm cannon. Each cluster of data symbols is the result of four shots. The zero angle coincides with the projectile flight path.

The solid and dashed lines in the figure correspond to calculations made with the Abel and perfect gas equations, respectively. The projectile base pressure for this cannon is less than 300 atmospheres so the covolume term in the Abel equation had only a modest effect on the results. The predictions are generally in good agreement with the data. The only exception occurs at the 10-degree position with the brake in place.

The results in Figure 8 are for the 105-mm cannon. In this case, the base pressure is near 800 atmospheres and the value of using the Abel equation is evident. The predictions lie somewhat above the data forward of the muzzle, but this is not a characteristic of the model. The comparison in Figure 9 for the 120-mm cannon and a base pressure of 660 atmospheres, shows more satisfactory agreement at these locations.

Of some concern is the tendency of the model to underpredict the data at the 150-degree location for both large cannon. The experimental peak may be due to a wave reflected off the ground or the vehicle. The cause is being investigated.

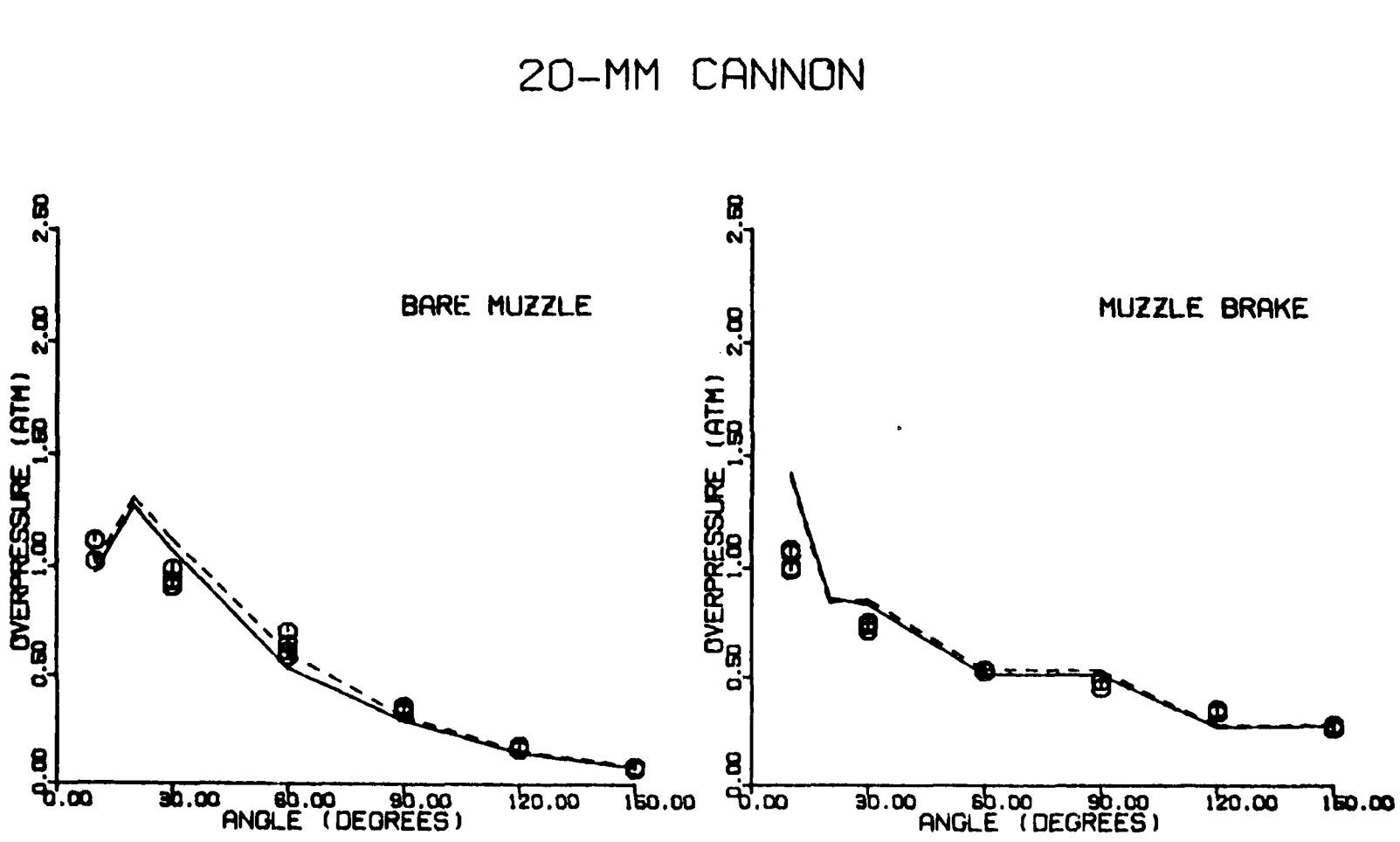

Figure 7. Comparison of model predictions with experimental free field overpressure data for the 20-mm cannon.

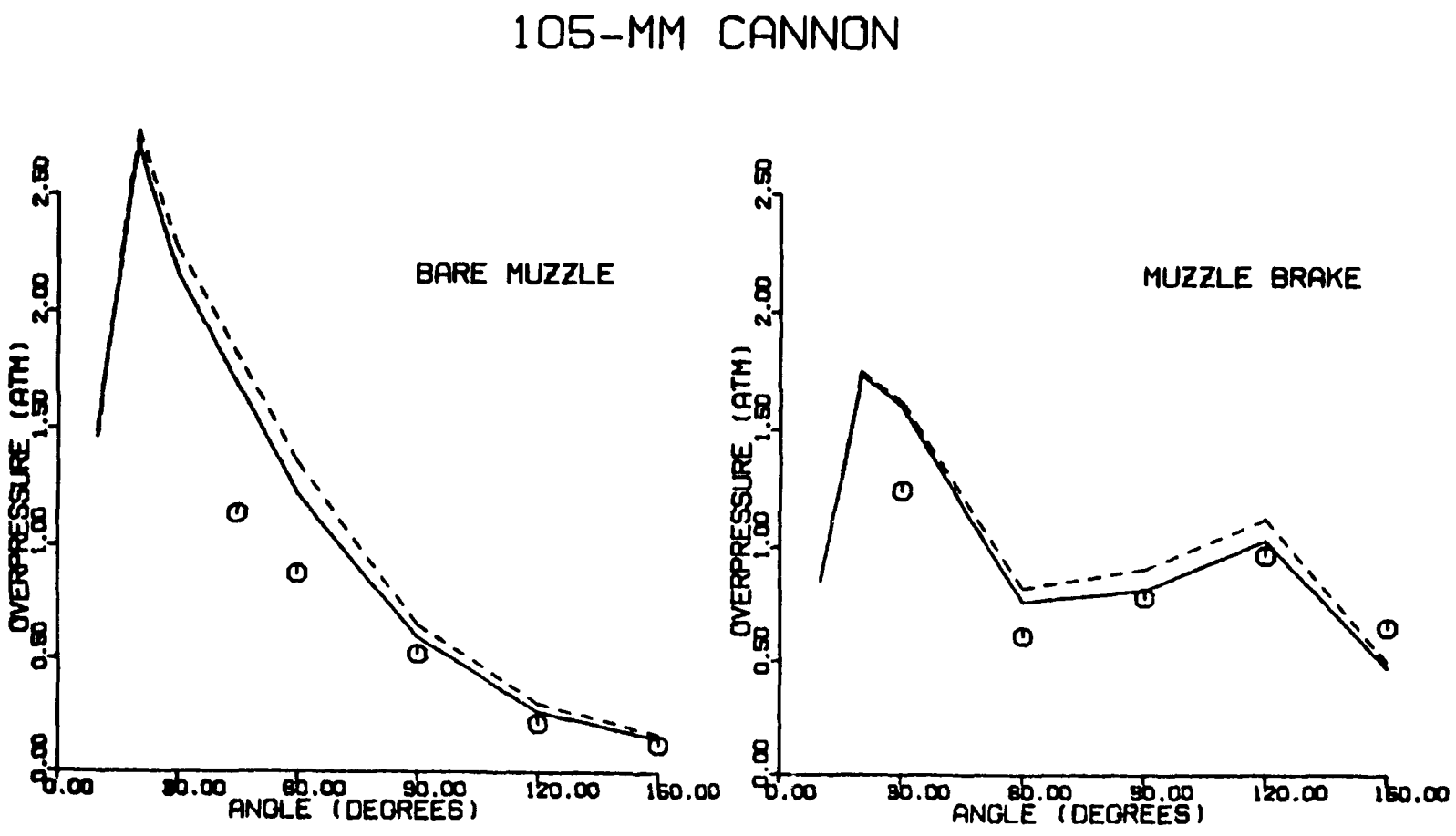

Figure 8. Comparison of model predictions with experimental free-field overpressure data for the 105-mm cannon.

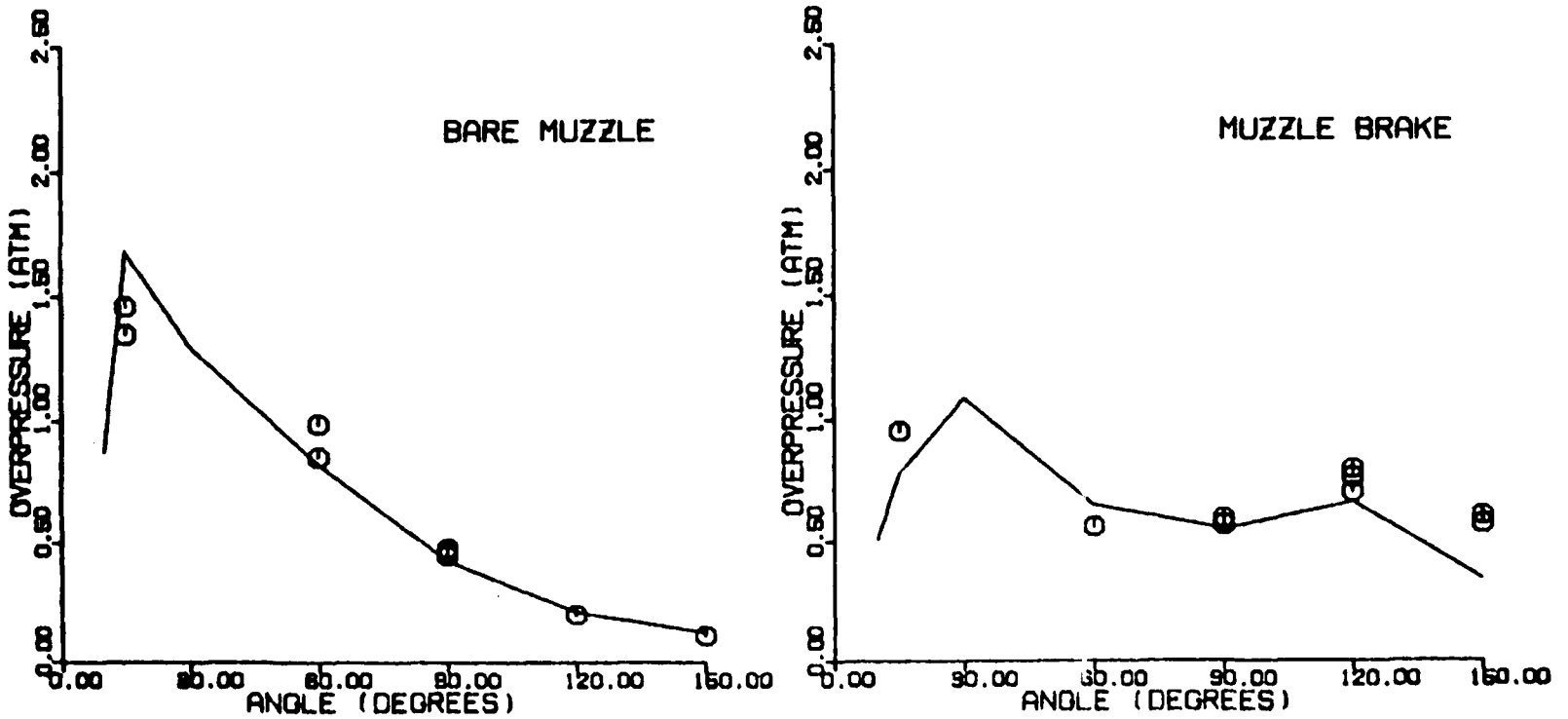

Figure 9. Comparison of model predictions with experimental free-field overpressure data for the 120-mm cannon.

Note that, in general, the peak overpressure is somewhat lower near the projectile flight path and rises to a maximum farther off axis. This can be explained by reference to the contour plots. Near the axis, the disturbance is influenced by the relatively weak projectile bow wave. Farther off axis, the disturbance is due to the strongest part of the main blast wave. The only exception occurs in the 20-mm brake case where the gage nearest the axis is struck directly by the main blast wave because of its position relative to the exit plane of the brake extension.

The overpressure plots for the large cannon indicate that venting decreases the strength of the blast wave downstream of the muzzle and increases it upstream. For the 20-mm cannon, the reduction downstream was not as pronounced, which is again associated with the brake extension. In a design situation, the tube will have to be lengthened somewhat to maintain the desired muzzle velocity, but the addition will be less than the vented length because the projectile continues to accelerate through this region. The trend of the overpressure measurements will then lie somewhat intermediate between the extremes observed here. In any event, the upstream pressure levels will increase. A method to limit the rise is discussed in the next section.

BLAST REDUCTION NEAR THE BREECH

In the experiments, all of the vents were located near the muzzle. The question arises, "Could another arrangement reduce the blast levels near the breech without producing significant changes in weapon impulse or projectile velocity?" Several patterns have been considered.

The obvious choice, increasing the vent spacing to spread the brake disturbance over a larger area, raised the pressure levels at the breech significantly. Displacing so many of the vents upstream simply moves the source of the

disturbance closer to the area of concern.

The most successful change involved moving just one or two rows of vents upstream while leaving the remaining vents at the muzzle. Overpressure predictions are shown in Figure 10 for the region aft of the muzzle of a 105-mm cannon at a 50-caliber radius (a different round was used in these calculations than the one described above). The bare muzzle data, represented by the square symbols, decrease monotonically from muzzle to breech. Adding 12 rows of vents near the muzzle produces the opposite trend, as indicated by the circles. Displacing two of these rows ten calibers upstream from the muzzle produces a significant reduction in blast near the breech, as indicated by the triangles.

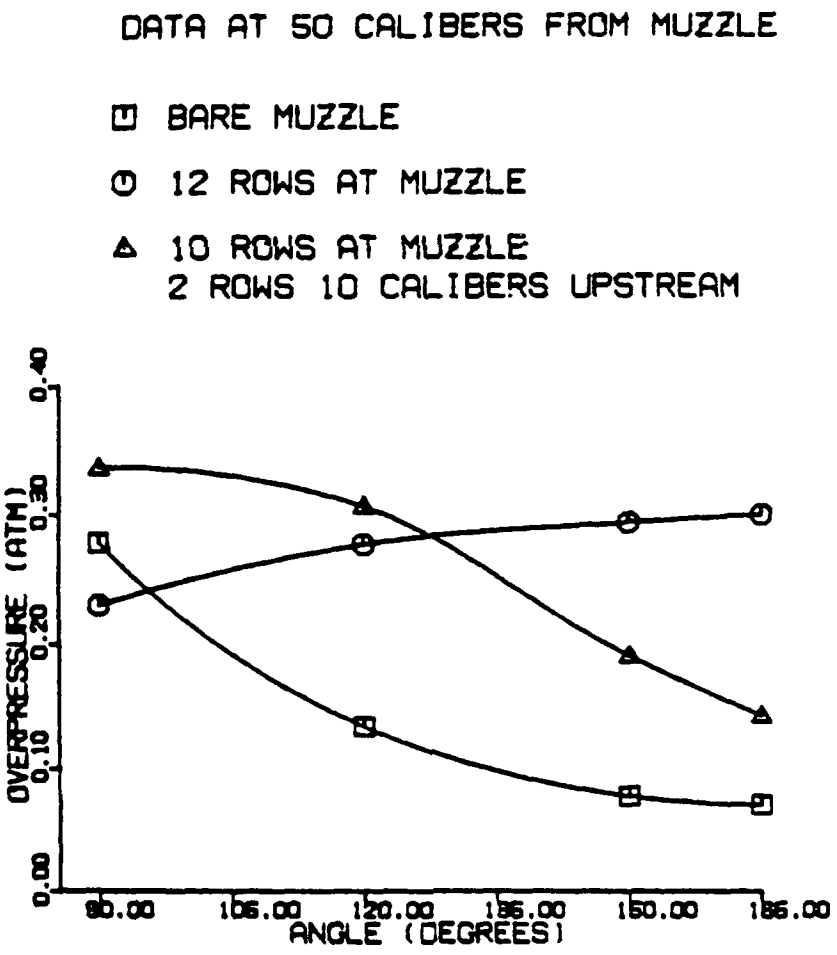

Figure 10. Overpressure predictions aft of the muzzle of a 105-mm cannon at a 50-caliber radius.

The scheme appears to work for two reasons. First, because only a small number of vents are moved upstream, the blast wave produced by them is relatively weak. Secondly, the flow field associated with them interferes with the propagation of the blast wave produced by the remaining vents. The result is that two waves arrive at the breech rather than one. By moving the right number of vents the correct distance from the muzzle, the strength of each wave can be minimized.

As noted above, a vented tube must be somewhat longer to maintain the desired projectile velocity. Displacing some of the vents upstream adds another fraction of a caliber. However, because the upstream vents work at a higher pressure level, fewer vents are required to match the impulse reduction obtained with the unsplit design. In the example above, only 11 rows are needed rather than the original 12.

The scheme will be tested in the laboratory using a 20-mm cannon and in the field using a 105-mm cannon. More complete details of the calculations will be given in a future report when the test results become available.

CONCLUSIONS

The model predictions are in satisfactory agreement with available overpressure data for small and large caliber cannon. The covolume correction in the Abel equation significantly improves the results for the latter. More data will be available in the near future for further comparison.

Upstream venting shows considerable promise as a method of reducing blast levels in the breech area while maintaining specified values of projectile velocity and weapon impulse. Laboratory and field testing of the scheme are planned.

REFERENCES

1. Dillon, R.E. Jr., "A Parametric Study of Perforated Muzzle Brakes," Technical Report ARLCB-TR-84015, Benet Weapons Laboratory, Watervliet, NY, May 1984.

2. Dillon, R.E. Jr., "Wall Thickness and Vent Area Effects on Perforated Muzzle Brake Performance," Technical Report ARLCB-TR-84020, Benet Weapons Laboratory, Watervliet, NY, May 1984.

3. Dillon, R.E. Jr. and Nagamatsu, H.T., "An Experimental Study of Perforated Muzzle Brakes," Technical Report ARLCB-TR-84004, Benet Weapons Laboratory, Watervliet, NY, February 1984.

4. Dillon, R.E. Jr. and Nagamatsu, H.T., "A Method of Analyzing Perforated Muzzle Brake Performance," Technical Report ARLCB-TR-84002, Benet Weapons Laboratory, Watervliet, NY, February 1984.

5. Dillon, R.E. Jr. and Nagamatsu, H.T., "An Experimental Study of Perforated Muzzle Brakes," AIAA Paper 84-1642, presented at the AIAA 17th Fluid Dynamics, Plasma Dynamics, and Lasers Conference, June 25-27, 1984, Snowmass, Colorado.

6. Nagamatsu, H.T., Choi, K.Y., Duffy, R.E., and Carofano, G.C., "An Experimental and Numerical Study of the Flow Through a Vent Hole in a Perforated Muzzle Brake," Technical Report ARCCB-TR-87016, Benet Laboratories, Watervliet, NY, June 1987.

7. Nagamatsu, H.T., Choi, K.Y., and Duffy, R.E., "Wall Thickness and Flow Mach Number Effects on Pressure Distribution in the Vent Hole for Perforated Muzzle Brakes," ARDEC Contractor Report ARCCB-CR-86038, Rensselaer Polytechnic Institute, Troy, NY, November 1986.

8. Carofano, G.C., "The Gasdynamics of Perforated Muzzle Brakes," Technical Report ARCCB-TR-88006, Benet Laboratories, Watervliet, NY, February 1988.

9. Carofano, G.C., "The Blast Field Produced by a Cannon Having a Perforated Muzzle Brake," Technical Report ARCCB-TR-88043, Benet Laboratories, Watervliet, NY, December 1988.

10. Corner, J., Theory of the Interior Ballistics of Guns, John Wiley and Sons, New York, 1950.

11. Plostins, P. and Clay, W.H., "Performance of Lightweight 105-mm Cannon Designs" (U), Technical Report BRL-TR-2749, Ballistic Research Laboratory, Aberdeen Proving Ground, MD, July 1986.

12. Baur, E.H. and Savick, D.S., "120-mm Perforated Muzzle Brake Performance," Ballistic Research Laboratory, Aberdeen Proving Ground, MD, technical report to be published.

13. Harten, A., "High Resolution Schemes for Hyperbolic Conservation Laws," J. Computational Physics, Vol. 49, No. 3, March 1983, pp. 357-393.

14. Carofano, G.C., "Blast Computation Using Harten's Total Variation Diminishing Scheme," Technical Report ARLCB-TR-84029, Benet Weapons Laboratory, Watervliet, NY, October 1984.

TECHNICAL REPORT INTERNAL DISTRIBUTION LIST

	NO. OF COPIES
CHIEF, DEVELOPMENT ENGINEERING DIVISION	
ATTN: SMCAR-CCB-D	1
-DA	1
-DC	1
-DI	1
-DP	1
-DR	1
-DS (SYSTEMS)	1
CHIEF, ENGINEERING SUPPORT DIVISION	
ATTN: SMCAR-CCB-S	1
-SE	1
CHIEF, RESEARCH DIVISION	
ATTN: SMCAR-CCB-R	2
-RA	1
-RE	1
-RM	1
-RP	1
-RT	1
TECHNICAL LIBRARY ATTN: SMCAR-CCB-TL	5
TECHNICAL PUBLICATIONS & EDITING SECTION ATTN: SMCAR-CCB-TL	3
DIRECTOR, OPERATIONS DIRECTORATE ATTN: SMCWV-OD	1
DIRECTOR, PROCUREMENT DIRECTORATE ATTN: SMCWV-PP	1
DIRECTOR, PRODUCT ASSURANCE DIRECTORATE ATTN: SMCWV-QA	1

NOTE: PLEASE NOTIFY DIRECTOR, BENET LABORATORIES, ATTN: SMCAR-CCB-TL, OF ANY ADDRESS CHANGES.

TECHNICAL REPORT EXTERNAL DISTRIBUTION LIST

	NO. OF COPIES
ASST SEC OF THE ARMY RESEARCH AND DEVELOPMENT ATTN: DEPT FOR SCI AND TECH THE PENTAGON WASHINGTON, D.C. 20310-0103	1
ADMINISTRATOR DEFENSE TECHNICAL INFO CENTER ATTN: DTIC-FDAC CAMERON STATION ALEXANDRIA, VA 22304-6145	12
COMMANDER US ARMY ARDEC	
ATTN: SMCAR-AEE	1
SMCAR-AES, BLDG. 321	1
SMCAR-AET-O, BLDG. 351N	1
SMCAR-CC	1
SMCAR-CCP-A	1
SMCAR-FSA	1
SMCAR-FSM-E	1
SMCAR-FSS-D, BLDG. 94	1
SMCAR-IMI-I (STINFO) BLDG. 59	2
PICATINNY ARSENAL, NJ 07806-5000	
DIRECTOR US ARMY BALLISTIC RESEARCH LABORATORY ATTN: SLCBR-DD-T, BLDG. 305 ABERDEEN PROVING GROUND, MD 21005-5066	1
DIRECTOR US ARMY MATERIEL SYSTEMS ANALYSIS ACTV ATTN: AMXSY-MP ABERDEEN PROVING GROUND, MD 21005-5071	1
COMMANDER HQ, AMCCOM ATTN: AMSMC-IMP-L ROCK ISLAND, IL 61299-6000	1

	NO. OF COPIES
COMMANDER ROCK ISLAND ARSENAL ATTN: SMCRI-ENM ROCK ISLAND, IL 61299-5000	1
DIRECTOR US ARMY INDUSTRIAL BASE ENGR ACTV ATTN: AMXIB-P ROCK ISLAND, IL 61299-7260	1
COMMANDER US ARMY TANK-AUTMV R&D COMMAND ATTN: AMSTA-DDL (TECH LIB) WARREN, MI 48397-5000	1
COMMANDER US MILITARY ACADEMY ATTN: DEPARTMENT OF MECHANICS WEST POINT, NY 10996-1792	1
US ARMY MISSILE COMMAND REDSTONE SCIENTIFIC INFO CTR ATTN: DOCUMENTS SECT, BLDG. 4484 REDSTONE ARSENAL, AL 35898-5241	2
COMMANDER US ARMY FGN SCIENCE AND TECH CTR ATTN: DRXST-SD 220 7TH STREET, N.E. CHARLOTTESVILLE, VA 22901	1
COMMANDER US ARMY LABCOM MATERIALS TECHNOLOGY LAB ATTN: SLCMT-TML (TECH LIB) WATERTOWN, MA 02172-0001	1

NOTE: PLEASE NOTIFY COMMANDER, ARMAMENT RESEARCH, DEVELOPMENT, AND ENGINEERING CENTER, US ARMY AMCCOM, ATTN: BENET LABORATORIES, SMCAR-CCB-TL, WATERVLIET, NY 12189-4050, OF ANY ADDRESS CHANGES.

TECHNICAL REPORT EXTERNAL DISTRIBUTION LIST (CONT'D)

	NO. OF COPIES
COMMANDER US ARMY LABCOM, ISA ATTN: SLCIS-IM-TL 2800 POWDER MILL ROAD ADELPHI, MD 20783-1145	1
COMMANDER US ARMY RESEARCH OFFICE ATTN: CHIEF, IPO P.O. BOX 12211 RESEARCH TRIANGLE PARK, NC 27709-2211	1
DIRECTOR US NAVAL RESEARCH LAB ATTN: MATERIALS SCI & TECH DIVISION CODE 26-27 (DOC LIB) WASHINGTON, D.C. 20375	1 1
DIRECTOR US ARMY BALLISTIC RESEARCH LABORATORY ATTN: SLCBR-IB-M (DR. BRUCE BURNS) ABERDEEN PROVING GROUND, MD 21005-5066	1
COMMANDER AIR FORCE ARMAMENT LABORATORY ATTN: AFATL/MN EGLIN AFB, FL 32542-5434	1
COMMANDER AIR FORCE ARMAMENT LABORATORY ATTN: AFATL/MNF EGLIN AFB, FL 32542-5434	1
METALS AND CERAMICS INFO CTR BATTELLE COLUMBUS DIVISION 505 KING AVENUE COLUMBUS, OH 43201-2693	1

NOTE: PLEASE NOTIFY COMMANDER, ARMAMENT RESEARCH, DEVELOPMENT, AND ENGINEERING CENTER, US ARMY AMCCOM, ATTN: BENET LABORATORIES, SMCAR-CCB-TL, WATERVLIET, NY 12189-4050, OF ANY ADDRESS CHANGES.